Enhancing the sustainability of household Fe^0/sand filters by using bimetallics and MnO_2.

Noubactep Chicgoua *[(1,2)], Caré Sabine.[(3)], Btatkeu K. Brice Donald.[(4)],

Nanseu-Njiki Charles Péguy [(5)]

[(1)] Angewandte Geologie, Universität Göttingen, Goldschmidtstraße 3, D - 37077 Göttingen, Germany;

[(2)] Kultur und Nachhaltige Entwicklung CDD e.V., Postfach 1502, D - 37005 Göttingen, Germany;

[(3)] Université Paris-Est, Laboratoire Navier, (ENPC/IFSTTAR/CNRS), 2 allée Kepler, 77420 Champs sur Marne, France.

[(4)] ENSAI/University of Ngaoundere, BP 455 Ngaoundere, Cameroon;

[(5)] Laboratoire de Chimie Analytique, Faculté des sciences, Université de Yaoundé I, B.P. 812 Yaoundé, Cameroon.

* corresponding author: e-mail: cnoubac@gwdg.de; Tel. +49 551 39 3191, Fax: +49 551 399379

(accepted Mon, 20 Jun 2011 13:06:39)

Abstract

Filtration systems containing metallic iron as reactive medium (Fe^0 beds) have been intensively used for water treatment during the last two decades. The sustainability of Fe^0 beds is severely confined by two major factors: (i) reactivity loss as result of the formation of an oxide scale on Fe^0, and (ii) permeability loss due to pore filling by generated iron corrosion products. Both factors are inherent to iron corrosion at pH > 4.5 and are common during the lifespan of a Fe^0 bed. It is of great practical significance to improve the performance of Fe^0 beds by properly addressing these key factors. Recent studies have shown that both reactivity loss and permeability loss could be addressed by mixing Fe^0 and inert materials. For a non porous additive like quartz, the threshold value for the Fe^0 volumetric proportion is 51 %. Using the Fe^0/quartz system as reference, this study theoretically discusses the possibility of (i) replacing Fe^0 by bimetallic systems (e.g. Fe^0/Cu^0), or (ii) partially replacing quartz by a reactive metal oxide (MnO_2 or TiO_2) to improve the efficiency of Fe^0 beds. Results confirmed the suitability of both tools for sustaining Fe^0 bed performance. It is shown that using a Fe^0:MnO_2 system with the volumetric proportion 51:49 will yield a filter with 40 % residual

30 porosity at Fe^0 depletion (MnO_2 porosity 62 %). This study improves Fe^0 bed design and can
31 be considered as a basis for further refinement and detailed research for efficient Fe^0 filters.
32 **Keywords**: Iron filters; Long-term reactivity; Oxide scale; Water treatment, Zerovalent iron.
33

34 ## 1 Introduction

35 A filtration system containing metallic iron as reactive medium (hereafter termed as Fe^0 bed)
36 is an attractive method which can continuously remove contaminants from surface water,
37 groundwater, and industrial effluent. The technology was introduced around 1990 by
38 Canadian hydrogeologists [1-3]. The Fe^0 bed technology has the potential to produce safe
39 drinking water in water plants [4-6], and to treat wastewater [4,7-9] and groundwater
40 [3,10,11]. Drawbacks for this innovative technology include (i) the accumulation of reaction
41 by-products, (ii) the decrease in surface activity over time (reactivity loss), and (iii) the
42 decrease of the bed permeability over the time (permeability loss) [11,12]. If Fe^0 beds are
43 used for above ground safe drinking water production, none of these three drawbacks is really
44 a problem. In fact, individual beds will be replaced as soon as a problem is observed.
45 Fe^0 beds have been demonstrated and used as an efficient and affordable technology for safe
46 drinking water production at small scale (household and small community) [13-21]. The first
47 generation filters made up of a 100 % layer of Fe^0 were very efficient but not sustainable
48 because of too rapid clogging [13,16]. The second generation filters used Fe^0 and inert filling
49 materials (mostly sand) and could achieve certain sustainability [19,22,23]. Recently, a
50 theoretical discussion on the proportion of Fe^0 in Fe^0 beds has been performed [24-26].
51 Results demonstrated that the Fe^0 volumetric ratio for sustainable filters is ≤ 52 % when the
52 additive is non porous (e.g. quartz). This threshold value does not give any information on the
53 nature of Fe^0 (e.g. bimetallic, composite). The nature of filling materials has been discussed
54 on the porosity perspective [25]. It is of great practical value to improve the performance of
55 Fe^0 beds. The following three perspectives could be addressed: (i) developing reliable Fe^0

56 materials (including composites), (ii) selecting the most suitable additive (porous, inert or/and
57 reactive), and (iii) optimizing Fe^0 bed design (e.g. thickness of a bed).
58 The suitability of plated metal (bimetallic systems) for reactivity enhancement has already
59 been demonstrated [27-29]. By plating a Fe^0 material with a more noble metal, the number of
60 micro-defects in the crystal lattice due to different dimensions and charges of micro-alloyed
61 elements, related to Fe^0 increase. Micro-alloyed components generate defects in a metal
62 structure (interstitials and vacancies in crystal lattice) and an imbalance in the charge
63 distribution, as a result of many micro-galvanic cells. These defects decrease energy barriers
64 for transport of Fe^{2+} ion from metal to oxide layer [27]. A positive accompanying effect is an
65 increase in ionic and electronic conductivity and thus, an increase of corrosion rate ([27] and
66 ref. cited therein). This makes the plated Fe^0 chemically much more reactive than the original
67 Fe^0 material. Contaminant removal by bimetallic systems is based on several physico-
68 chemical processes and the in situ formation of very reactive iron hydoxides. The major
69 processes in a Fe^0 bed are adsorption, co-precipitation and size exclusion.
70 The ability of MnO_2 to sustain contaminant removal by Fe^0 was indirectly demonstrated in a
71 recent study by He and Hering [30]. The authors demonstrated that As^{III} was quantitatively
72 oxidized to As^V by MnO_2 but resulted As^V remained in solution. Quantitative As removal was
73 indeed observed in systems containing Fe^{II} and was mostly attributed to As co-precipitation
74 with Fe^{III} hydroxides. In a similar way, MnO_2 can sustain Fe^0 oxidative dissolution yielding
75 Fe^{II} which capability to induce reductive dissolution of MnO_2 will sustain the process of
76 contaminant removal. Note that the work of He and Hering [30] recalled that “contaminant
77 reduction” and “contaminant removal” should never be randomly interchanged. In other
78 words, a chemical transformation (oxidation or reduction) may favour contaminant removal
79 but is not a stand alone removal mechanism. Aqueous contaminant removal by co-
80 precipitation with in-situ generated metal hydroxides is well documented process for all
81 classes of contaminants ([29, 31] and ref. therein).

The present study intends to theoretically discuss the optimization of Fe^0 bed by two different tools: (i) replacing Fe^0 by a bimetallic system, and (ii) using MnO_2 as reactive additives, e.g. partially or totally substituting quartz by MnO_2 in a reference Fe^0/quartz bed. Both tools have the potential to improve the contaminant removal efficiency and prolong the lifespan of Fe^0 beds. For the sake of clarity, the process of contaminant removal in Fe^0 beds will be first presented.

2 Contaminant removal in Fe^0 filters

2.1 Filtration in packed-column

A Fe^0 bed is primarily a packed-column of granular Fe^0 and quartz (sand) particles. The efficiency of packed-columns for contaminant removal is usually evaluated by monitoring the time dependent evolution of (i) the contaminant concentration in the effluent, and (ii) the water velocity through the column. Physical and chemical conditions evaluated in such experiments include grain particle size and shape, solution pH, solution ionic strength and composition [32,33]. Ideally, contaminants are deposited throughout the entire filter media. Accordingly, Fe^0 filtration is a deep-bed or depth filtration process [34].

2.2 Filtration in a Fe^0 bed

Contaminant removal within a Fe^0/quartz filter is not comparable to contaminant removal by an adsorption column [5,35]. The most important feature of Fe^0/quartz filters regards the specificity of the removal process. In an adsorption column, contaminants with different physico-chemical properties can be separated due to their differential affinity to the adsorbing material (e.g. activated carbon, iron oxide). Similarly, particles with different sizes can be separated in a depth sand filter. But in a Fe^0/quartz filter, there is primarily no such specificity as contaminants are removed during the dynamic process of iron corrosion products formation (Fe hydroxides/oxides) and by resulted Fe hydroxides/oxides [35, 36].

2.3 Mechanism of contaminant removal in Fe^0/sand filters

107 Regardless from any contaminant inflow, the initial pore space in a Fe^0/quartz filter is
108 progressively filled by in situ generated Fe hydroxides/oxides. Decreased pore space is
109 coupled to improved size exclusion capacity. Accordingly, regardless from physico-chemical
110 interactions between contaminants, Fe^0 and Fe hydroxides/oxides, contaminant removal by
111 pure size exclusion will inevitably occur with increasing service life. This fundamental aspect
112 has received little attention to date as the scientific community was focused on specific
113 interactions between selected contaminants and Fe^0. In this effort a particular attention was
114 paid to chemical reduction [10,11].
115 It has already been demonstrated that contaminants are fundamentally entrapped within the
116 film of corrosion products in the vicinity of the Fe^0 surface [37-40]. It is essential to note that
117 the formation of corrosion products is a cycle of expansion/contraction occurring in the pore
118 space [5,26,35]. During this process, native iron (Fe^0: SSA < 1 m^2/g) is first transformed to
119 voluminous iron hydroxides possibly having specific surface area (SSA) > 500 m^2/g before
120 progressively contracted to amorphous and crystalline oxides with SSA ≤ 10 m^2/g. The
121 voluminous colloid which is intermediary formed [41] during an expansion/contraction cycle
122 can be compared to a spider web which traps inflowing contaminants and keeps them
123 adsorbed while the colloid is further transformed. In other words, before the pore space
124 becomes close enough for the Fe^0 filter to act as an ultra-filtration system, the
125 expansion/contraction cycle traps contaminants from the infiltrating water. It is certain, that
126 the kinetics of iron oxidation will decrease as soon as not enough space is available for
127 expansive corrosion. This is a plausible explanation for the controversial observation, that
128 TCE removal rates were higher in a system with 85 % Fe^0 than they were in a 100 % Fe^0
129 (w/w) system [42]. Substituting a fraction of Fe^0 by sand (quartz) was proven a prerequisite
130 for efficient long-term permeable Fe^0 filters [24,25]. The present study aims at theoretically
131 discussing the substitution of a portion of quartz in the dual media (Fe^0/quartz) by a reactive

132 oxide to sustain long-term Fe^0 reactivity. A further discussed way to sustain Fe^0 reactivity is
133 to plate Fe^0 by a second more electropositive metal.

134 ## 3 Sustaining Fe^0 reactivity

135 The presentation above has suggested that successful contaminant removal in a Fe^0/quartz bed
136 is coupled with the whole process of iron corrosion. Accordingly, a reliable way to warrant
137 continuous contaminant removal is to sustain iron corrosion. This section examines two
138 possibilities of sustaining Fe^0 corrosion.

139 ### 3.1 Use of bimetallics

140 The deposition of small amounts of second metals such as Ni and Pd onto the Fe^0 surface has
141 been proven beneficial for the process of aqueous contaminant removal ([12] and ref. therein).
142 Bimetallic systems are an efficient media for accelerating the decontamination [27-29]. The
143 prevailing operating mode of bimetallic systems [12] was recently challenged. It was shown
144 that any enhanced contaminant reduction, if applicable, occurs by an indirect process [43].
145 Table 1 summarises the standard electrode potentials of seven elemental metals (Me^0) which
146 may be used to sustain Fe^0 oxidation in filters: Co^0, Ni^0, Cu^0, Ag^0, Pd^0, Pt^0, Au^0. From these
147 metals, Cu^0 is the most used.

148 An ideal Me^0 acts as a catalyst. For example, Cu^0 is oxidized by water to Cu^{2+} and the
149 resulted Cu^{2+} oxidizes Fe^0. Considering Me^0 as pure catalyst, calculated amounts of Fe^0/Me^0
150 will be added to a sand filter and the porosity will vary as in a Fe^0/quartz bed. In other words,
151 replacing Fe^0 particles by bimetallic (Fe^0/Me^0) particles of similar size and occupying the
152 same volume will not significantly impact porosity loss. Bimetallic/quartz filters will behave
153 like Fe^0/quartz filters in term of the evolution of the porosity but exhibit an enhanced long-
154 term reactivity. The theoretical evolution of porosity loss due to clogging is discussed in
155 section 4.

156 ### 3.2 Use of metal oxides

157 The use of natural oxides to sustain Fe^0 reactivity was derived from the well-documented
158 reductive dissolution of MnO_2 by Fe^{II} [46,47]. This process was successfully used to
159 demonstrate the importance of corrosion products in the process of contaminant removal by
160 Fe^0 [48-52]. Moreover, the reductive dissolution of MnO_2 by Fe^{II} is a well-established
161 hydrometallurgical process [53-55]. Recently, Bafghi et al. [55] published a work on the
162 reductive dissolution of manganese ore in the presence of Fe^0. Based on theoretical and
163 experimental facts, they concluded that Fe^0 was superior to Fe^{II} for MnO_2 reductive
164 dissolution. However, they insisted on the fact that Fe^{II} is more available. Mechanistic details
165 will not be considered here as it is sufficient to consider that metal oxides could sustain Fe^0
166 corrosion (Tab. 2, Tab. 3). Remember that contaminants are fundamentally removed by iron
167 corrosion products (adsorption and co-precipitation) and these are increasingly available when
168 iron oxidation is sustained by Fe^{II} consumption [51,52,56].
169 Only the four naturally abundant oxides will be considered: Al_2O_3, MnO_2, SiO_2 and TiO_2
170 (Tab. 2). The standard electrode potentials from Tab. 2 show that only MnO_2 and TiO_2 could
171 sustain Fe^0 reactivity. Accordingly, Al_2O_3 and SiO_2 can only be used as inert filling materials.
172 The ability of MnO_2 to sustain Fe^0 corrosion was already demonstrated [48-50,56]. In
173 particular, the success of SONO Arsenic Filters in Bangladesh is based on continuous
174 production of reactive iron oxides by the used manganese oxide/Fe^0 composite (coupled to
175 size exclusion in the filter). Table 3 depicts some relevant electrode reactions (half-reactions)
176 for the discussion of the Fe^0 reactivity. From Tab. 3 it can be seen that MnO_2 is theoretically
177 by far superior to TiO_2 in sustaining Fe^0 corrosion. However, the suitability of available metal
178 oxides to sustain Fe reactivity should be tested on the case-by-case basis. Moreover, the
179 objective should not be to use the most reactive metal oxide but rather the one with
180 satisfactorily reactivity for individual purposes. For example, for a given Fe^0, a very reactive
181 MnO_2 can accelerate the Fe^0 corrosion in such a way that filter fouling/clogging is achieved
182 similar as with bio-corrosion [10,11]. In such situations a lesser reactive MnO_2 should be

183 used. Testing well-characterized Fe^0 and reactive manganese oxides in various proportions is
184 regarded as a tool to produce site-specific composites. In fact, the composite currently used in
185 SAF filters is the same material which is used everywhere (actually mostly in Bangladesh and
186 Nepal) [14,18]. However, contaminated waters are of various background compositions and
187 each water could be treated with appropriate composites.
188 To discuss the evolution of the pore space within the filter as metal oxides react, it will be
189 considered that MnO_2 and TiO_2 reduction at neutral pH values mostly yield insoluble
190 hydroxides: MnOOH and TiOOH (Eq. 17 and Eq. 18).
191 $Fe^0 + 3\ MnO_2 + 2\ H_2O \Leftrightarrow FeOOH + 3\ MnOOH$ (17)
192 $Fe^0 + 3\ TiO_2 + 2\ H_2O \Leftrightarrow FeOOH + 3\ TiOOH$ (18)
193 Eq. 17 and 18 suggest that the oxidation of one Fe atom consumes three molecules of the
194 adsorbent MnO_2 (or TiO_2) and produces one FeOOH and three MnOOH (or three TiOOH) as
195 new adsorbents. The volume variation is estimated based on values of the specific weight
196 defined as the ratio of the molecular volume of the reaction products to the molecular volume
197 of the educts (Tab. A3). The discussion will only concern MnO_2 because no tabulated value
198 could be found for TiOOH. The evolution of the porosity loss due to clogging is discussed in
199 section 4.

200 ## 4 Evolution of the residual porosity using bimetallic particles or metal oxides

201 This section will start with some general design equations. It has been recently showed that
202 dimensionless design equations could be written such that for each practical case the
203 appropriate values are derived [24-26]. In other words, the same equations are applied to
204 household Fe^0 filters, Fe^0 treatment trench, and Fe^0 reactive walls. In each case, the used
205 materials (Fe^0 and additives) should be thoroughly characterized. Relevant material
206 characteristics include porosity, particle size, shape, specific weight, and surface area. The
207 impacts of material characteristics on the bed efficiency are not discussed here.

208 ### 4.1 General design equations of Fe^0 beds

209 Cylindrical beds are considered. H is the height and D is the internal diameter. The cylinder
210 contains a reactive zone with the height H_{rz} and the volume V_{rz}. Beds are supposed to be filled
211 by granular materials. The compactness (or packing density) C (-) is defined as the ratio of the
212 volume of the particles to the total packing volume (V_{rz}). Considering the granular material as
213 composed of mono-dispersed spheres subjected to soft vibrations, the compactness C is
214 generally considered to be equal to 0.64 for a random close packing. It is assumed that the
215 particles are non porous.
216 The initial porosity Φ_0 (-) of the reactive zone and the thickness H_{rz} of the reactive zone are
217 respectively then given by:

218 $$\Phi_0 = 1 - C \qquad (19)$$

219 $$H_{rz} = \frac{4}{\pi D^2} \cdot V_{rz} \qquad (20)$$

220 The filling of the bed porosity by iron corrosion products can be estimated from a simplified
221 modeling (Fig. 1) based on the following assumptions:
222 (i) uniform corrosion: the radius reduction of the spherical particles is the same for all the Fe^0
223 particles.
224 (ii) the packing density C remains constant for all particles (Fe^0 and quartz). The volume of
225 the granular material is not modified by the corrosion process: no pressure induced by rust
226 formation around Fe particles and no compaction of the Fe^0 mixture during the corrosion
227 process (V_{rz} remains constant).
228 (iii) reaction products are fluid enough to progressively fill available pore space.
229 Assuming that the coefficient of volumetric expansion or the specific volume (η) of the
230 reaction products is:

231 $$\eta = V_{oxide}/V_{Fe} \qquad (21)$$

where V_{oxide} is the volume of the reaction product and V_{Fe} the volume of the parent Fe^0. It is assumed that Fe_3O_4 is the sole iron corrosion product for the Fe/quartz system. The specific volume for Fe_3O_4 is 2.1.

The surplus volume of the reaction products contributing to porosity loss is V'_{oxide}. Per definition V'_{oxide} is the difference between the volume V_{oxide} of reaction products and the volume V_{Fe} of parent Fe^0. V'_{oxide} is given by Eq. 22:

$$V'_{oxide} = (\eta - 1) * V_{Fe} \quad (22)$$

Assuming that iron expansive corrosion is the sole clogging factor, the bed is clogged when the volume V'_{oxide} is equal to the initial inter-granular voids ($\Phi_0.V_{rz}$), the volume $V_{Fe,clogging}$ of the consumed Fe^0 leading to clogging of the bed is then estimated by:

$$V_{Fe,clogging} = \frac{\Phi_0 \cdot V_{rz}}{\eta - 1}. \quad (23)$$

Eq. 23 is of fundamental importance for Fe^0 bed design as it determines the ideal Fe^0 volume (and thus Fe^0 mass) to be used. If V_0 is the initial volume of dense Fe^0, three cases can be distinguished:

"(i) $V_{Fe,clogging} > V_0$, no clogging due to expansive iron corrosion will occur. In this case, the real volume of Fe which may be consumed ($V_{consumed\text{-}Fe}$) is equal to the initial volume V_0 of Fe ($V_{consumed\text{-}Fe} = V_0 < V_{Fe,clogging}$) and there is a residual porosity at Fe^0 depletion ($\Phi_r \neq 0$);

(ii) $V_{Fe,clogging} = V_0$, clogging will not occur before Fe^0 depletion ($V_{consumed\text{-}Fe} = V_{Fe,clogging} = V_0$) but the final porosity is zero ($\Phi_r = 0$):

(iii) $V_{Fe,clogging} < V_0$, clogging will occur before Fe^0 depletion ($\Phi_r = 0$). In this case, the real volume of consumed Fe leading to clogging is inferior to the initial volume V_0 of Fe ($V_{consumed\text{-}Fe} = V_{Fe,clogging} < V_0$) and the excess Fe^0 amount should be regarded as pure material wastage [24]."

256 The residual porosity Φ_r defined by $\Phi_r = V_{residual\ voids}/V_{rz}$ and the residual mass of the iron
257 (Fe^0) are evaluated by Eq. 24 and Eq.25:

258 $$\Phi_r = \Phi_0 - (\eta - 1).\frac{V_{consumed-Fe}}{V_{rz}} \quad (24)$$

259 $$\frac{M}{M_0} = \frac{V_0 - V_{consumed-Fe}}{V_0} \quad (25)$$

260 where V_0 is the initial volume of Fe, $V_{consumed\text{-}Fe}$ is the volume of the Fe which is consumed
261 and M is the actual mass of Fe given by $M = \rho_{Fe}*(V_0 - V_{consumed\text{-}Fe})$ with ρ_{Fe} = 7,800 kg/m^3.
262 When the clogging appears before depletion of Fe^0, the volume $V_{consumed\text{-}Fe}$ is given by the Eq.
263 24 and the residual porosity is $\Phi_r = 0$ and there is a residual mass of iron $M/M_0 \neq 0$ (Eq. 25).
264 When there is no clogging, the volume $V_{consumed\text{-}Fe} \leq V_0$ and $\Phi_r \neq 0$ (Eq. 24) and the Fe^0 mass
265 at Fe^0 depletion is zero ($M/M_0 = 0$; Eq. 25).
266 Eq. 19 through 25 should be routinely used to design laboratory experiments, pilot and field
267 works.

268 **4.2 Case of bimetallic/quartz system**

269 To sustain the Fe^0 reactivity, Fe particles are replaced by bimetallic particles of comparable
270 particle sizes. For Fe^0/Cu^0 bimetallic particles with 7 % in mass of Cu, the volumetric
271 proportion of Fe^0 is 93.85 % (considering for specific weights ρ_{Fe}= 7800 kg/m^3 and ρ_{Cu}= 8960
272 kg/m^3) and the reaction product is Fe_3O_4. The residual porosity and the residual mass are
273 given by the same equations by replacing the initial volume V_0 of Fe^0 by 93.85 %* V_0. The
274 results for the Fe^0/quartz and the bimetallic/quartz systems are given in Fig. 1. The trends are
275 similar for both cases. While decreasing the Fe^0 proportion at constant reactive zone
276 thickness, Fe^0 depletion was achieved for Fe^0/quartz systems > 51 vol-% Fe^0. In the case of
277 bimetallic/quartz system (Fe^0/Cu^0), the clogging is avoided for < 54 vol-% bimetallic.
278 To further sustain the efficiency of Fe^0 beds, bimetallic systems containing larger amounts of
279 plating metals (Me^0) could be used. Moreover composites should be manufactured and tested.

280 Those composites should contain uniformly distributed Me^0 in the bulk of Fe^0 materials and
281 not just deposited at their surface. Apart from such bulk composites, special Fe^0 materials
282 with higher contents in S for instance, could be manufactured and tested. In fact, during the
283 steel making process, efforts target as completely remove S are made. Sulphur is known for
284 its negative effect on corrosion resistance of steel. However, in the context of water treatment
285 with Fe^0, readily corrosive Fe^0 may be suitable.

286 **4.3.1 Case of Fe^0/MnO_2/quartz system**

287 A reference reactive zone is considered as made up of 51 vol-% Fe^0 and 49 vol-% quartz as it
288 allows avoiding the clogging before Fe^0 depletion as shown in Fig. 1. Iron filings from
289 Gotthart Maier Metallpulver GmbH (Rheinfelden, Germany) containing 92 % Fe^0 (w/w) is
290 used for the calculations. Quartz particles of similar particle size are replaced by MnO_2
291 particles in order to increase Fe^0 reactivity. In presence of MnO_2, it is assumed that chemical
292 reactions yield to FeOOH and MnOOH products (Eq. 17). When MnO_2 particles have been
293 consumed, the Fe corrosion process leads to the reaction products Fe_3O_4.

294 Calculations made with characteristics of a natural MnO_2 (ϕ_{Mno2} = 62 %) given by Li et al.
295 [57] are used in this study (Tab. A.1 and A.2). The mineral contained (weight) 77.8 % MnO_2,
296 2.7 % Fe, 0.87 % Si, 2.78 % Al and 0.01 % S. For simplifications, it is considered that the
297 mineral is made up of 77.8 % MnO_2 and 22.2 % of a "gangue" having the characteristic of
298 quartz (inert and non porous). This assumption was the rationale to use the specific weight of
299 quartz in estimating the volumetric expansion coefficient for MnO_2 (Appendix). Calculations
300 showed that for the reference system (vol. Fe:quartz = 51:49), less than 3 % Fe^0 is necessary
301 to consume the amount of MnO_2 that could be contained in up to 49 vol-% MnO_2, when
302 quartz is completely replaced by MnO_2. Moreover, it is shown that thanks to the porosity of
303 MnO_2, there is a net increase of the initial bed porosity in comparison to the Fe^0/quartz bed.
304 Furthermore, because the chemical transformation (Fe + MnO_2) to (MnOOH +FeOOH) was

not expansive but slightly compressive ($\eta = 0.94$), there is a net increase of the residual bed porosity (Appendix).

Eq. 24 and 25 are slightly modified because the initial porosity Φ_0 is increased by the internal porosity of the MnO_2 particles and the voids ($\Phi_0.V_{rz}$) are filled by (i) the MnOOH hydroxides with $\eta_1 = V_{MnOOH}/V_{MnO2} = 0.94$ (Appendix), (ii) the FeOOH hydroxides with $\eta_2 = V_{FeOOH}/V_{Fe} = 3.03$ and (iii) Fe_3O_4 with $\eta_3 = V_{Fe3O4}/V_{Fe} = 2.1$. Values of η_2 and η_3 are from ref. [58].

The initial porosity Φ_0, the residual porosity Φ_r and the residual mass of the iron (Fe^0) are evaluated by Eq. 26 , Eq. 27 and Eq.28:

$$\Phi_0 = (1 - C) + f_{Mno2} * \phi_{Mno2} \quad (26)$$

$$\Phi_r = \Phi_0 - \frac{(\eta_1 - 1).V_1 + (\eta_2 - 1).V_2 + (\eta_3 - 1).V_3}{V_{rz}} \quad (27)$$

$$\frac{M}{M_0} = \frac{V_0 - V_2 - V_3}{V_0} \quad (28)$$

Where ϕ_{MnO2} is the internal porosity of the MnO_2 particles ($\phi_{MnO2} = 62$ %) and f_{pp} (-) is the porous particle volume fraction determined by $f_{pp} = V_{Mno2}/V_{MnO2}$ with V_{MnO2} the volume of the porous particles MnO_2. V_1 is the volume of the dense MnO_2, V_2 is the Fe^0 volume which reacts with MnO_2. The volume of Fe^0 (V_2) is obtained considering that one Fe atom consumes three molecules of MnO_2 (Eq. 17). V_3 is the volume of Fe^0 leading to Fe_3O_4 after MnO_2 depletion.

At Fe depletion ($M/M_0 = 0$), the residual porosity Φ_r is given by Eq. 27 ($V_3 = V_0 - V_2$ with V_0 the initial volume of Fe^0 in the reactive zone). If clogging appears before depletion of Fe^0, the residual porosity is $\Phi_r = 0$ and the residual mass is given by Eq. 28.

The evolution of the initial and residual porosity is given in Fig. 2a for the reference system when the volumetric proportion of MnO_2 varies from 0 to 49 %. Thanks to the internal porosity of MnO_2 the initial porosity (Φ_0) increased from 36.0 to 55.4 %. On the other hand,

328 Fe^0 depletion was observed in all systems but the residual porosity varies from 8.3 to 40.6 %.
329 The increase of the residual porosity with increasing MnO_2 proportion is due to two factors:
330 (i) the internal porosity of MnO_2 and (ii) the light volumetric compaction of MnO_2 reduction
331 to MnOOH. Remember that in the reference system the residual porosity is zero at Fe^0
332 depletion. Therefore, similarly as for the Fe^0/pumice system [25,59], the internal porosity of
333 MnO_2 could be regarded as storage room for in situ generated corrosion products (see also
334 Appendix). In summary, MnO_2 reduction to MnOOH has two beneficial effects: (i) sustaining
335 Fe^0 reactivity and (ii) serving as storage room for corrosion products. Additionally, the
336 chemical potential of the reaction between Fe^{II} and MnO_2 will drive the diffusion of Fe^{II} from
337 Fe^0 oxidative dissolution to the internal surface of MnO_2. Thus, filling the internal porosity of
338 MnO_2 with iron corrosion products is more likely to occur than for an inert material like
339 pumice. Another important aspect is that Mn^{II} from the reductive dissolution of MnO_2 will
340 migrate in the system and be oxidized by several species to MnOOH or MnO_2 [60-62] which
341 will further oxidize Fe^{II} from Fe^0. Accordingly, despite stoichiometric disadvantage, MnO_2
342 may work as catalyst to sustain Fe^0 reactivity during its whole lifespan [63,64].
343 The fact that no pore clogging was observed for 51 vol-% Fe^0 suggests that more Fe^0 could be
344 used for the same bed (V_{rz} constant). In this case, the volume of MnO_2 is necessarily reduced.
345 Fig. 2b shows the results of systems with volumetric ratios Fe^0:MnO_2 varying between 60:0
346 and 60:40. That is, when quartz is progressively replaced by MnO_2. While the initial porosity
347 increased from 36 to 51.9 %, the residual porosity increased from 0.0 to 24.8 %. This results
348 show clearly that even in rising the Fe^0 volumetric ratio in the column from 51 to 60 %, a
349 residual porosity exists and the Fe^0 performance is increased by the cycle of MnO_2 as
350 described above.

351 **5 Concluding remarks**

352 A Fe^0/quartz filter is regarded as an assisted slow sand filtration system which efficiency is
353 improved by addition of a calculated amount of metallic iron [65]. The aqueous corrosion by

354 infiltrating raw water should ideally transform the initial Fe^0 filter to an efficient filtration
355 system. Improved filtration efficiency is based on the volumetric expansive nature of iron
356 corrosion [59,66] which ideally only partly fills initial pore space in the sand-like filter [67].
357 This communication is part of an ongoing effort for low-cost water treatment using well-
358 design Fe^0 beds [5,6,17,24-26,68,69]. While dual filters of Fe^0 and quartz will be long-term
359 permeable, the substitution of Fe^0 by bimetallic materials or the substitution of inert sand by
360 reactive metal oxides will sustain long-term reactivity. For example, sustaining Fe^0 reactivity
361 by substituting a fraction of Fe^0 by metallic copper chips or (partly or entirely) replacing sand
362 by granulated MnO_2 will help to design efficient and sustainable filtration systems. The
363 encouraging results of SONO filters in Bangladesh [14,15,18,70-72] suggest that practitioners
364 of subsurface permeable barriers should check the possibility of replacing Fe^0 by composites
365 or amended Fe^0 by reactive additives. The concept presented and discussed in this
366 communication (and related articles) would be useful in designing efficient and affordable
367 water filtration systems at several scales. The concept also renders itself as a basis for further
368 refinement and detailed research at laboratory and field scale. One may wonder how the Fe^0
369 bed technology will be developed in different parts of the world.

370 **Acknowledgments**

371 Dr. Boniface P. T. Fokwa (Institute of Inorganic Chemistry, RWTH Aachen University) is
372 acknowledged for fruitful discussions on the mineralogy of manganese oxides. The
373 manuscript was improved by the insightful comments of anonymous reviewers from CLEAN
374 Soil, Air, Water.

375 **References**

376 [1] G.W. Reynolds, J.T. Hoff, R.W. Gillham, Sampling bias caused by materials used to
377 monitor halocarbons in groundwater, *Environ. Sci. Technol*. **1990**, 24, 135.
378 [2] S.F. O´Hannesin, R.W. Gillham, Long-term performance of an in situ "iron wall" for
379 remediation of VOCs, *Ground Water* **1998**, 36, 164.

380 [3] R.W. Gillham, Development of the granular iron permeable reactive barrier technology
381 (good science or good fortune), In "*Advances in environmental geotechnics : proceedings of*
382 *the International Symposium on Geoenvironmental Engineering in Hangzhou, China,*
383 *September 8-10, 2009*"; Y. Chen, X. Tang, L. Zhan (Eds); Springer Berlin/London, **2010**, 5–
384 15.
385 [4] D.D.J. Antia, Sustainable zero-valent metal (ZVM) water treatment associated with
386 diffusion, infiltration, abstraction and recirculation, *Sustainability* **2010,** 2, 2988.
387 [5] C. Noubactep, Metallic iron for safe drinking water worldwide. *Chem. Eng. J*. **2010**, 165,
388 740.
389 [6] C. Noubactep, A. Schöner, Metallic iron: dawn of a new era of drinking water treatment
390 research? *Fresen. Environ. Bull*. **2010**, 19, 1661.
391 [7] S. Junyapoon Use of zero-valent iron for wastewater treatment, KMITL Sci. Tech. J.
392 **2005**, 5, 587.
393 [8] G. Bartzas, K. Komnitsas, I. Paspaliaris, Laboratory evaluation of Fe^0 barriers to treat
394 acidic leachates, Miner. Eng. **2006,** 19, 505.
395 [9] K. Komnitsas, G. Bartzas, K. Fytas, I. Paspaliaris, Long-term efficiency and kinetic
396 evaluation of ZVI barriers used for clean up of copper containing solutions, *Miner. Eng*. **2007**,
397 20, 1200.
398 [10] M.M. Scherer, S. Richter, R.L. Valentine, P.J.J. Alvarez, Chemistry and microbiology of
399 permeable reactive barriers for in situ groundwater clean up, Crit. Rev. *Environ. Sci. Technol*.
400 **2000**, 30, 363.
401 [11] A.D. Henderson, A.H. Demond, Long-term performance of zero-valent iron permeable
402 reactive barriers: a critical review, *Environ. Eng. Sci*. **2007**, 24, 401.
403 [12] C.-c. Lee, R.-a Doong, Concentration effect of copper loading on the reductive
404 dechlorination of tetrachloroethylene by zerovalent silicon, *Water Sci. Technol*. **2010**, 62, 28.

405 [13] A.H. Khan, S.B. Rasul, A.K.M. Munir, M. Habibuddowla, M. Alauddin, S.S. Newaz, A.
406 Hussam, Appraisal of a simple arsenic removal method for groundwater of Bangladesh, *J.*
407 *Environ. Sci. Health*, **2000**, A35, 1021.
408 [14] A. Hussam, A.K.M. Munir, A simple and effective arsenic filter based on composite iron
409 matrix: Development and deployment studies for groundwater of Bangladesh, *J. Environ. Sci.*
410 *Health* **2007**, A 42, 1869.
411 [15] T.K.K. Ngai, R.R. Shrestha, B. Dangol, M. Maharjan, S.E. Murcott, Design for
412 sustainable development – Household drinking water filter for arsenic and pathogen treatment
413 in Nepal, *J. Environ. Sci. Health* **2007**, A 42, 1879.
414 [16] A. Hussam, Contending with a development disaster: SONO filters remove arsenic from
415 well water in Bangladesh, *Innovations* **2009**, 4, 89.
416 [17] C. Noubactep, A. Schöner, P. Woafo, Metallic iron filters for universal access to safe
417 drinking water, *Clean: Soil, Air, Water* **2009**, 37, 930.
418 [18] D. Pokhrel, B.S. Bhandari, T. Viraraghavan, Arsenic contamination of groundwater in
419 the Terai region of Nepal: An overview of health concerns and treatment options, *Environ.*
420 *Int*. **2009**, 35, 157.
421 [19] A.M. Gottinger, *Chemical-free arsenic removal from potable water with a ZVI-amended*
422 *biofilter*. Master thesis, University of Regina (Saskatchewan, Canada) **2010**, 90 pp.
423 [20] A.M. Gottinger, D.J. Wild, D. McMartin, B. Moldovan, D. Wang, Development of an
424 iron-amended biofilter for removal of arsenic from rural Canadian prairie potable water. In:
425 Water Pollution X. A.M. Marinov and C.A. Brebbia, Eds.; WIT Press: Ashurst, Southampton
426 **2010**, 333.
427 [21] M.I. Litter, M.E. Morgada, J. Bundschuh, Possible treatments for arsenic removal in
428 Latin American waters for human consumption, *Environ. Pollut*. **2010**, 158, 1105.
429 [22] O.X. Leupin, S.J. Hug, Oxidation and removal of arsenic (III) from aerated groundwater
430 by filtration through sand and zero-valent iron, *Water Res.* **2005**, 39, 1729.

[23] O.X. Leupin, S.J. Hug, A.B.M. Badruzzaman, Arsenic removal from Bangladesh tube well water with filter columns containing zerovalent iron filings and sand, *Environ. Sci. Technol.* **2005**, 39, 8032.

[24] C. Noubactep, S. Caré, F. Togue-Kamga, A. Schöner, P. Woafo, Extending service life of household water filters by mixing metallic iron with sand, *Clean: Soil, Air, Water* **2010**, 38, 951.

[25] C. Noubactep, S. Caré, Enhancing sustainability of household water filters by mixing metallic iron with porous materials, *Chem. Eng. J*. **2010**, 162, 635.

[26] C. Noubactep, S. Caré, Dimensioning metallic iron beds for efficient contaminant removal, *Chem. Eng. J.* **2010**, 163, 454.

[27] A. Bojic, M. Purenovic, D. Bojic, Removal of chromium(VI) from water by micro-alloyed aluminium based composite in flow conditions. *Water SA* **2004**, 30, 353.

[28] A. Bojic, M. Purenovic, D. Bojic, T. Andjelkovic, Dehalogenation of trihalomethanes by a micro-alloyed aluminium composite under flow conditions. *Water SA* **2007**, 33, 297.

[29] A. Bojic, D. Bojic, T. Andjelkovic, Removal of Cu^{2+} and Zn^{2+} from model wastewaters by spontaneous reduction–coagulation process in flow conditions, *J. Hazard. Mater.* **2009**, 168, 813.

[30] Y.T. He, J.G. Hering, Enhancement of Arsenic(III) Sequestration by Manganese Oxides in the Presence of Iron(II). *Water Air Soil Pollut.* **2009**, 203, 359.

[31] K. Eusterhues, T. Rennert, H. Knicker, I. Kgel-Knabner, K.U. Totsche, U. Schwertmann, Fractionation of organic matter due to reaction with ferrihydrite: Coprecipitation versus adsorption. *Environ. Sci. Technol.* **2010,** doi: 10.1021/es1023898.

[32] N. Tufenkji, Modeling microbial transport in porous media: Traditional approaches and recent developments. *Adv. Water Res.* **2007**, 30, 1455.

455 [33] G.J. Williams, B. Sheikh, R.B. Holden, T.J. Kouretas, K.L. Nelson, The impact of
456 increased loading rate on granular media, rapid depth filtration of wastewater, *Water Res.*
457 **2007**, 41, 4535.
458 [34] D.D. Putnam, M.A. Burns, Predicting the filtration of noncoagulating particles in depth
459 filters, *Chem. Eng. Sci*. **1997**, 52, 93.
460 [35] C. Noubactep, The suitability of metallic iron for environmental remediation. *Environ.*
461 *Progr. Sust. En*. **2010**, 29, 286.
462 [36] C. Noubactep, An analysis of the evolution of reactive species in Fe^0/H_2O systems. *J.*
463 *Hazard. Mater.* **2009**, 168, 1626.
464 [37] C. Noubactep, Processes of contaminant removal in "Fe^0–H_2O" systems revisited: The
465 importance of co-precipitation, *Open Environ. J.* 1 **2007**, 9.
466 [38] C. Noubactep, A critical review on the mechanism of contaminant removal in Fe^0–H_2O
467 systems, *Environ. Technol*. **2008**, 29, 909.
468 [39] C. Noubactep, The fundamental mechanism of aqueous contaminant removal by metallic
469 iron. *Water SA* **2010**, 36, 663.
470 [40] C. Noubactep, A. Schöner, M. Sauter. Significance of oxide-film in discussing the
471 mechanism of contaminant removal by elemental iron materials, In "Photo-Electrochemistry
472 & Photo-Biology for the Sustainablity"; S. Kaneco, B. Viswanathan, H. Katsumata (Eds.),
473 Bentham Science Publishers, **2010**, 1, 35
474 [41] J. Livage, J. Lemerle, Transition metal oxide gels and colloids, *Ann. Rev. Mater. Sci.*
475 **1982**, 12,103.
476 [42] E. Bi, J.F. Devlin, B. Huang, Effects of mixing granular iron with sand on the kinetics of
477 trichloroethylene reduction, *Ground Water Monit. Remed*. **2009**, 29, 56.
478 [43] C. Noubactep, On the operating mode of bimetallic systems for environmental
479 remediation, *J. Hazard. Mater*. **2009**, 164, 394.

480 [44] Y. Gerasimov, V. Dreving, E. Eremin, A. Kiselev, V. Lebedev, G. Panchenkov, A.
481 Shlygin, *Physical Chemistry*, vol. 2, MIR Moscow **1985**, 624 pp.
482 [45] K.B. Krauskopf, D.K. Bird, *Introduction to geochemistry*, Third Edition, McGraw-Hill,
483 Inc, New York **1995**, 647 pp.
484 [46] D.F.A. Koch, Kinetics of the reaction between manganese dioxide and ferrous ion, *Austr.*
485 *J. Chem*. **1957**, 10, 150.
486 [47] D. Postma, C.A.J. Appelo, Reduction of Mn-oxides by ferrous iron in a flow system:
487 column experiment and reactive transport modelling, *Geochim. Cosmochim. Acta* **2000**, 64,
488 1237.
489 [48] C. Noubactep, G. Meinrath, P. Dietrich, B. Merkel, Mitigating uranium in groundwater:
490 Prospects and limitations, *Environ. Sci. Technol*. **2003**, 37, 4304.
491 [49] C. Noubactep, G. Meinrath, J.B. Merkel, Investigating the mechanism of uranium
492 removal by zerovalent iron materials, *Environ. Chem*. **2005**, 2, 235.
493 [50] C. Noubactep, A. Schöner, G. Meinrath, Mechanism of uranium (VI) fixation by
494 elemental iron, *J. Hazard. Mater*. **2006**, 132, 202.
495 [51] A. Ghauch, H. Abou Assi, A. Tuqan, Investigating the mechanism of clofibric acid
496 removal in Fe^0/H_2O systems, *J. Hazard. Mater*. **2010**, 176, 48.
497 [52] A. Ghauch, H. Abou Assi, S. Bdeir, Aqueous removal of diclofenac by plated elemental
498 iron: bimetallic systems, J. Hazard. Mater. **2010**, 182, 64.
499 [53] K. Inoue, M. Okui, M. Tanaka, K. Shinoda, S. Suzuki, Y. Waseda, Influence of
500 manganese on iron oxyhydroxides and oxides formed in aqueous solution, *Corros. Sci*. **2008**,
501 50, 811.
502 [54] M.J. Lottering, L. Lorenzen, N.S. Phala, J.T. Smit, G.A.C. Schalkwyk, Mineralogy and
503 uranium leaching response of low grade South African ores, *Miner. Eng*. **2008**, 21, 16.
504 [55] M.Sh. Bafghi, A. Zakeri, Z. Ghasemi, M. Adeli, Reductive dissolution of manganese ore
505 in sulfuric acid in the presence of iron metal, *Hydrometallurgy* **2008**, 90, 207.

506 [56] D. Burghardt, A. Kassahun, Development of a reactive zone technology for simultaneous
507 in situ immobilisation of radium and uranium, *Environ. Geol.* **2005**, 49, 314.
508 [57] K. Li, R.R. Rothfus, A.H. Adey, Effect of macroscopic properties of manganese oxides
509 on absorption of sulfur dioxide. *Environ. Sci. Technol*. **1968**, 2, 619.
510 [58] S. Caré, Q.T. Nguyen, V. L'Hostis, Y. Berthaud, Mechanical properties of the rust layer
511 induced by impressed current method in reinforced mortar, *Cement Concrete Res.* **2008**, 38,
512 1079.
513 [59] N. Moraci, P.S. Calabrò, Heavy metals removal and hydraulic performance in zero-
514 valent iron/pumice permeable reactive barriers. *J. Environ. Manag.* **2010**, 91, 2336.
515 [60] T. Kohler, T. Armbruster, E. Libowitzky, Hydrogen Bonding and Jahn–Teller Distortion
516 in Groutite,α-MnOOH, and Manganite, γ-MnOOH, and Their Relations to the Manganese
517 Dioxides Ramsdellite and Pyrolusite. *J. Solid State Chem*. **1997**, 133, 486.
518 [61] J.E. Post, Manganese oxide minerals: Crystal structures and economic and environmental
519 significance. *Proc. Natl. Acad. Sci. USA* **1999**, 96, 3447.
520 [62] S.A. Kirillov, V.S. Aleksandrova, T.V. Lisnycha, D.I. Dzanashvili, S.A. Khainakov, J.R.
521 García, N.M. Visloguzova, O.I. Pendelyuk, Oxidation of synthetic hausmannite (Mn_3O_4) to
522 manganite (MnOOH). *J. Mol. Struct.* **2009**, 928, 89.
523 [63] T. Ohzuku, M. Kitagawa, T. Hirai, Electrochemistry of manganese dioxide in lithium
524 nonaqueous cell: III. X-Ray diffractional study on the reduction of spinel-related manganese
525 dioxide. *J. Electrochem. Soc*. **1990**, 137, 769.
526 [64] Y. Chabre, J. Pannetier, Structural and electrochemical properties of the proton / γ-MnO_2
527 system. *Progr. Solid State Chem*. **1995**, 23, 1.
528 [65] C. Noubactep, Metallic iron for safe drinking water production. *Freiberg Online*
529 *Geology*, 2011,. 27, 38 pp, ISSN 1434-7512. (www.geo.tu-freiberg.de/fog)
530

[66] K. Bhargava, A.K. Ghosh, Y. Mori, S. Ramanujam, Model for cover cracking due to rebar corrosion in RC structures, *Eng. Struct*. **2006**, 28, 1093.

[67] K.-M. Yao, M.T. Habibian, C.R. O'melia, Water and waste water filtration: concepts and applications. *Environ. Sci. Technol*. **1971**, 1105–1112.

[68] C. Noubactep, P. Woafo, Elemental iron (Fe^0) for better drinking water in rural areas of developing countries, In Merkel B.J., Hasche-Berger A. (Eds.) *Uranium in the Environment*. Springer, Berlin, Heidelberg **2008**, 121.

[69] C. Noubactep, S. Caré, Designing laboratory metallic iron columns for better result comparability. *J. Hazard. Mater*. **2011**, 189, 809–813.

[70] H. Chiew, M.L. Sampson, S. Huch, S. Ken, B.C. Bostick, Effect of groundwater iron and phosphate on the efficacy of arsenic removal by iron-amended biosand filters, *Enviro. Sci. Technol*. **2009**, 43, 6295.

[71] Md. Shafiquzzaman, Md.S. Azam, I. Mishima, J. Nakajima, Technical and social evaluation of arsenic mitigation in rural Bangladesh. *J. Health Pop. Nutr.*, **2009**, 27, 674.

[72] S. Tuladhar, L.S. Smith, SONO filter: An excellent technology for save water in Nepal. *SOPHEN* **2009**, 7, 18.

[73] R.M. Cornell, U. Schwertmann, *The iron oxides: structure, properties, reactions, occurrences, and uses*. 2nd ed., Wiley-VCH Weinheim **2003**, 613 pp.

[74] W.L. Roberts, T.J. Campbell, G.R. Rapp, *Encyclopedia of Minerals* (Second Edition). Chapman & Hall, New York **1990**, 980 pp.

552 **Table 1**: Relevant half-reactions for more electropositive metals likely to be added to sustain
553 iron corrosion in household filters with the relevant standard electrode potentials. Standard
554 electrode potentials are arranged in increasing order of E°. The higher the E° value, the
555 stronger the oxidative capacity for Fe^0. Standard electrode potentials are compiled from refs.
556 [44,45].
557

Reaction			E° (V)	Eq.
$Fe^{2+} + 2\ e^-$	$\Leftrightarrow$	Fe^0	-0.44	(1)
$Co^{2+} + 2\ e^-$	$\Leftrightarrow$	Co^0	-0.28	(2)
$Ni^{2+} + 2\ e^-$	$\Leftrightarrow$	Ni^0	-0.24	(3)
$Cu^{2+} + 2\ e^-$	$\Leftrightarrow$	Cu^0	0.33	(4)
$Ag^{+} + e^-$	$\Leftrightarrow$	Ag^0	0.80	(5)
$Pd^{2+} + 2\ e^-$	$\Leftrightarrow$	Pd^0	0.95	(6)
$Pt^{2+} + 2\ e^-$	$\Leftrightarrow$	Pt^0	1.18	(7)
$Au^{3+} + 3\ e^-$	$\Leftrightarrow$	Au^0	1.50	(8)

558
559

559 **Table 2**: Inventory of possible redox couples in the present study with the relevant standard
560 electrode potentials. Standard electrode potentials are compiled from ref. [56,57]. (*)
561 marked are values from wikipedia. Relevant redox couples are those which could
562 oxidize Fe^0 (E^0 > -0.44 V). Accordingly, only MnO_2 and TiO_2 are relevant.

Oxide	Species	Couples	E^0 (V)	Relevance
Al_2O_3	Al^0, Al^{III}	Al^{III}/Al^0	-1.67	No
MnO_2	Mn^0, Mn^{II}, Mn^{III}, Mn^{IV}	Mn^{II}/Mn^0	-1.18	No
		Mn^{III}/Mn^{II}	1.54	Yes
		Mn^{IV}/Mn^{II}	1.23	Yes
		Mn^{IV}/Mn^{III}	0.95(*)	Yes
SiO_2	Si^0, Si^{IV}	Si^{IV}/Si^0	-0.99	No
TiO_2	Ti^0, Ti^{III}, Ti^{IV}	Ti^{III}/Ti^0	-1.63(*)	No
		Ti^{IV}/Ti^{III}	0.19(*)	Yes
Fe_2O_3	Fe^0, Fe^{II}, Fe^{III}	Fe^{II}/Fe^0	-0.44	Yes
		Fe^{III}/Fe^{II}	0.77	Yes

563
564
565

565 **Table 3**: Relevant half-reactions for sustaining iron corrosion with the relevant standard
566 electrode potentials. Standard electrode potentials are arranged in increasing order
567 of E^0. The higher the E^0 value, the stronger the oxidative capacity for Fe^0.
568

Reaction			E^0 (V)	Eq.
$Fe^{2+} + 2\ e^-$	$\Leftrightarrow$	Fe^0	-0.44	(9)
$2\ H^+ + 2\ e^-$	$\Leftrightarrow$	H_2 (g)	0.00	(10)
$TiO_{2(s)} + 4\ H^+ + e^-$	$\Leftrightarrow$	$Ti^{3+} + 2\ H_2O$	0.19	(11)
$Fe^{3+} + e^-$	$\Leftrightarrow$	Fe^{2+}	0.77	(12)
$O_2 + 2\ H_2O + 4\ e^-$	$\Leftrightarrow$	$4\ OH^-$	0.81	(13)
$MnO_{2(s)} + 4\ H^+ + e^-$	$\Leftrightarrow$	$Mn^{3+} + 2\ H_2O$	0.95	(14)
$MnO_{2(s)} + 4\ H^+ + 2\ e^-$	$\Leftrightarrow$	$Mn^{2+} + 2\ H_2O$	1.23	(15)
$MnOOH_{(s)} + 3H^+ + e^-$	$\Leftrightarrow$	$Mn^{2+} + 2\ H_2O$	1.54	(16)

569
570
571

571 **Figure 1**

572

573

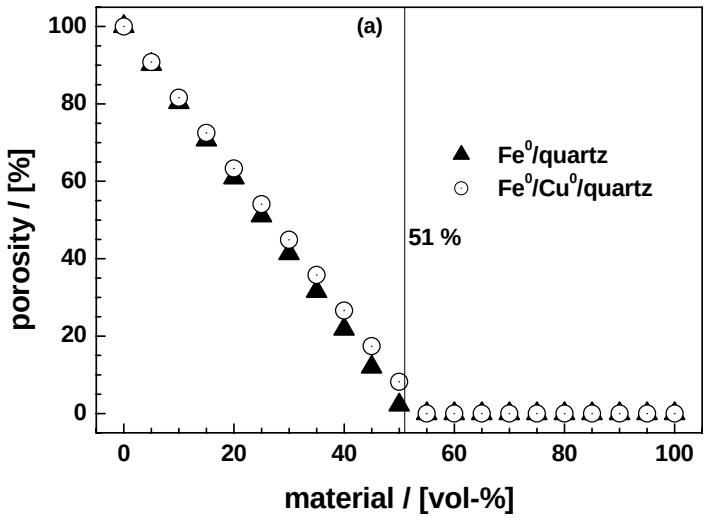

574

575

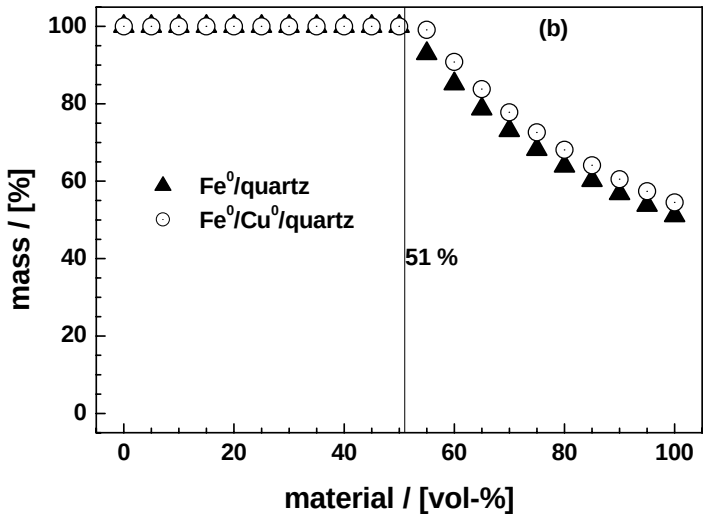

576

577

578

579

579 **Figure 2**:

580

581

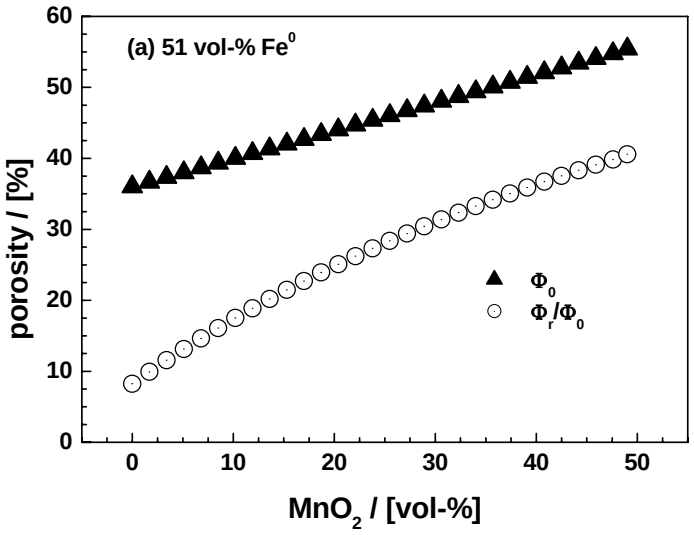

582

583

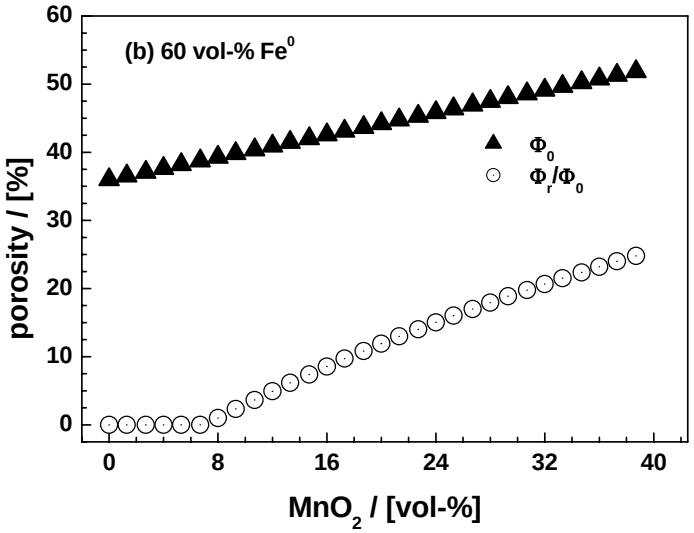

584

585

586

586 **Figure Captions**

587

588 **Figure 1**: Evolution of the residual porosity Φ_r/Φ_0 (%) (a) and the residual mass of Fe^0 M_r/M_0

589 (%) (b) versus the volumetric % ratio of material in the Fe^0 bed. It is clear that in both cases,

590 for Fe^0 > 51 vol-%, bed clogging will occur before Fe^0 depletion. For a 100 % Fe^0 bed, only

591 51 w-% of Fe^0 is consumed at bed clogging.

592

593 **Figure 2**: Evolution of the residual porosity versus the % replaced quartz particles by MnO_2

594 for 51 % Fe^0 (a) and 60 % Fe^0 (b). It is evident that replacing quartz by porous MnO_2 could

595 enable the use of a larger amount of Fe^0 in a bed.

596

597

Appendix

A.1 Estimation of the η-value for MnOOH

Table A.1 summarizes relevant characteristics of selected manganese oxides and Tab. A.2 gives the volume and the ratio of the volume of MnOOH to other oxides [73,74]. Apart from MnOOH, all oxides listed in Tab. A.1 may be considered as potential starting materials.

The volumetric contraction or expansion coefficient η expressed as the ratio of the volume of MnOOH to the volume of each oxide is determined according to:

$$\eta = V_{MnOOH}/V_{oxyde} = (M_{MnOOH}/\rho_{MnOOH})/(M_{oxide}/\rho_{oxide}) \quad (S1)$$

With M_i and ρ_i the mass and specific weight of the i species (MnOOH or oxide)

As the mass of MnOOH and the oxides can be expressed by $M_i = \mathbf{M_i} * n_i$ where $\mathbf{M_i}$ is the molecular weight and n_i is the number of mole of each species in the chemical reaction, the coefficient η is:

$$\eta = V_{MnOOH}/V_{oxyde} = (\mathbf{M}_{MnOOH} * n_{MnOOH}/\rho_{MnOOH})/(\mathbf{M}_{oxide} * n_{oxide}/\rho_{oxide}) \quad (S2)$$

It can be noticed that the specific weight is either measured or calculated according to:

$$\rho_i = (\mathbf{M}_i * Z)/(V_{i,cell} * A) \quad (S3)$$

Where Z is the formula unit per cell, V_{cell} is the volume of the unit cell and A the Avogadro number ($A = 6.023\ 10^{23}$).

The calculated densities of MnOOH and of the oxides are given in Tab A.2. A description of a natural a manganite (γ-MnOOH) from the Kalahari manganese field (South Africa) is given by Kohler et al. [60]. The crystal structure of that manganite was space group P21 /c, a = 5.304(1), b = 5.277(1), c = 5.304(1), β = 114.38(2)°, and Z = 4). A clear deviation from the values (a, b, c and β) tabulated by Roberts et al. [74] (Tab. A.2) gives nevertheless similar result for the density.

Table A.3 suggests that depending from the starting manganese oxide, there will be either a volumetric contraction or expansion (η-values). These results show that the initial material

should be well-characterized because the clogging of the filter will depend on the nature of the used oxide. For this reason, the characteristics of a natural MnO_2 mineral given by Li et al. [57] have been used in this work (Tab. A.4). The next section estimates the η-value for this natural mineral. Accordingly, each natural or synthetic mineral have to be properly characterized before used as an additive in Fe^0 beds.

628 **Table A.1**: Crystallographic characteristics (formula, crystal system, space group) and
629 expression of the volume of the unit cell for manganese oxide minerals.

Mineral	**Group**	**Formula**	**System**	$\mathbf{V_{unit\ cell}}$
Manganite	$B2_1/d$	MnOOH	Monoclinic	abc sin(β)
Pyrolusite	$P4_2/mmm$	MnO_2	Tetragonal	a^2c
Todorokite	P2/m	$(Mn,Ca,Mg)Mn^{IV}{}_3O_7.H_2O$	Monoclinic	abc sin(β)
Birnessite	-	MnO_2	Orthorhombic	abc
Hausmannite	$I4_1/amd$	$Mn^{II}Mn^{III}O_4$	Tetragonal	a^2c
Manganosite	Fm3m	MnO	Cubic	a^3
Psilomelane	C2/m	$BaMn^{II}Mn^{IV}{}_8O_{16}(OH)_4$	Monoclinic	abc sin(β)

630

631

631

632 **Table A.2**: Characteristics of selected manganese oxides. Apart from manganite* (Z = 4), all
633 values are from from Roberts et al. [74]. Data for manganite* are from Kohler et
634 al. [60].

Mineral	**Z**	**a**	**b**	**c**	**angle**	**density**	
	(-)	(Å)	(Å)	(Å)	β (°)	calc.	meas.
Manganite	8	8.94	5.28	5.74	90	4.30	4.33
Manganite*	4	5.304	5.277	5.304	114.38	4.31	-
Pyrolusite	2	4.42	4.42	2.87	-	5.148	5.06
Todorokite	3	9.75	2.84	9.59	90	3.49	3.66-3.82
Birnessite	3	8.54	15.39	14.29	-	3.0	3.87
Hausmannite	4	5.7621	5.7621	9.4696	-	4.84	4.84
Manganosite	4	4.436	4.436	4.436	-	5.364	5.365
Psilomelane	2	13.929	2.8459	9.678	92,39	6.45	-

635

636

637

637 **Table A.3**: Name, Formula, calculated density, molecular weight and η-values for the
638 manganese oxide minerals in Tab. A.2. η is ratio of the volume of MnOOH to the
639 volume of each oxide (here $n_{MnOOH} = n_{oxide.}$). If η > 1, there is an expansion; this is
640 theoretically the case when pyrolusite is used. For birnessite, a compaction is
641 predicted (η < 1). The η values will be slightly different with the measured density
642 but the trends will be similar.

Mineral	Formula	Calculated density	Molecular weight	η: specific volume
		kg/m^3	kg/mol	(-)
manganite	MnOOH	4310	0.08784	1
Birnessite	MnO_2	3000	0.08694	0.70
Pyrolusite	MnO_2	5148	0.08694	1.21

643

644

644 **Table A.4**: Selected properties of the natural manganese oxide used by Li et al. [57]. The
645 characteristics of pellets are used in this work.

646
647

Form	**Mn**	**Sp. gravity**	**Bulk density**	**porosity**	**SSA**
	(%)	(-)	(g/cm^3)	(%)	(m^2/g)
Pellet	53.5	3.58	1.35	0.62	14.9
Powder	53.5	3.58	2.05	0.43	12.2

648

649

A.2: Estimation of the volumetric expansion coefficient for natural MnO_2 mineral

A natural porous MnO_2 mineral with the bulk density ρ_{min}, a porosity ϕ_{min}, and a MnO_2 content x_{MnO2} is used. A mass (M_{min}) of this sample occupies a volume V_{min} given by:

$$V_{min} = V_{MnO2} + V_{gangue} + V_{void} \quad \text{(S4)}$$

Where V_{gangue} is the volume of the supposedly inert material (called gangue) that is disseminated in MnO_2 and represents a fraction of $(1 - x_{MnO2})$ of the mass of solid material. Accordingly, the mass of the mineral is given by:

$$M_{min} = M_{MnO2} + M_{gangue} \quad \text{(S5)}$$

Per definition, $V_{void} = \phi_{min} * V_{min}$ and S4 is read:

$$V_{MnO2} + V_{gangue} = V_{min}\,(1 - \phi_{min}) = (M_{min}/\rho_{min})*(1 - \phi_{min}) \quad \text{(S6)}$$

The task is to give an expression of V_{MnO2} as function of all known parameters. The relation between the mass of MnO_2 in the mineral (M_{MnO2}), the mass of the gangue (M_{gangue}) and the mass of the mineral (M_{min}) is given by:

$$M_{MnO2} = x_{MnO2} * M_{min},\ (x_{MnO2} < 1) \quad \text{(S7a)}$$

$$M_{gangue} = (1 - x_{MnO2}) * M_{min} \quad \text{(S7b)}$$

Per definition, $M_{min} = \rho_{min} * V_{min}$. This expression gives V_{min} which can be used in Eq. S6 to have $(V_{MnO2} + V_{gangue})$. Knowing the real volume occupied by MnO_2 and the gangue in the mineral, the open issue is to calculate the volume of MnOOH resulting from MnO_2.

The volume occupied by MnOOH is given by:

$$V_{MnOOH} = M_{MnOOH}/\rho_{MnOOH} = \mathbf{M}_{MnOOH} * n_{MnOOH}/\rho_{MnOOH} \quad \text{(S8a)}$$

$$V_{MnOOH} = \mathbf{M}_{MnOOH} * n_{MnOOH}/(\mathbf{M}_{MnOOH} * Z) * (V_{cell} * A) = (A/Z) * n_{MnOOH} * V_{cell} \quad \text{(S8b)}$$

Where A is the Avogadro constant ($6.023*10^{23}$), $n_{MnOOH} = M_{MnOOH}/87.84$; $\mathbf{M}_{MnOOH} = 87.84$ g/mol the molar weight of MnOOH, and V_{cell} the volume of the unit cell of MnOOH. It can be noticed that $n_{MnOOH} = n_{MnO2} = M_{MnO2}/86.94$; $\mathbf{M}_{MnO2} = 86.94$g/mol the molar weight of MnO_2.

The coefficient of volumetric compaction or expansion (η) is then given by the ratio $\eta = V_{MnOOH}/V_{MnO2}$. But one needs an approximation to evaluate V_{MnO2} in Eq. S3. One plausible approximation is to consider the gangue as quartz and deduce the volume V_{gangue} from the relation $M_{gangue} = \rho_{quartz}*V_{gangue}$. M_{gangue} is given by Eq. S4a.

$$V_{gangue} = M_{gangue}/\rho_{quartz} = (1 - x_{MnO2})*M_{min}/\rho_{quartz} \quad \text{(S9)}$$

So that the volume V_{MnO2} is given by:

$$V_{MnO2} = (M_{min}/\rho_{min})*(1 - \phi_{min}) - (1 - x_{MnO2})*M_{min}/\rho_{quartz} \quad \text{(S10)}$$

Illustration

The volumetric expansion coefficient used for Fig. 2 is calculated using 100 g of mineral having the characteristics of the pellets from Li et al. [57] (Tab. SI.3). The following values are given: ρ_{min} = 1.35 g/cm^3; ϕ_{min} = 0.62; x_{MnO2} = 0.778; M_{min} = 100 g; M_{gangue} = 22.8 g; M_{MnO2} = 77.8 g; ρ_{quartz} = 2.65 g/cm^3. Unit cell parameters for MnOOH: structure = monoclinic, a = 8.94, b = 5.28, c = 5.74 and $\beta = 90°$. $V_{cell} = a*b*c*\sin\beta$, Z=4.

77.8 g MnO_2 corresponds to 0.895 mole of MnO_2. The quantitative reduction will yield n_{MnOOH} = 0.895 mole.

After S3, $V_{MnO2} + V_{gangue} = M_{min}/\rho_{min}*(1 - \phi_{min}) = (100/1.35)*(1\text{-}0.62) = 28.15$ cm^3

After S9, $V_{gangue} = (1 - 0.778)*100/2.65 = 8.38$ cm^3

Accordingly, $V_{MnO2} = 28.15 - 8.38 =$ **19.77 cm^3 (V_{MnO2} = 19.77 cm^3)**

After S8b, $V_{MnOOH} = (A/4)*(M_{MnO2}/86{,}94)*V_{cell}$

$= (6.023*10^{23}/4)*0.895*1.35*10^{-22} =$ **18.59 cm^3 (V_{MnOOH} = 18.59 cm^3)**

The contraction coefficient η is then: **18.59** /19.77 = 0.94; **η = 0.94**.

This result means that when the 77.8 g of MnO_2 in the original mineral in consumed, the produced MnOOH occupies a volume of 0.94 * 19.77 = 18.59 cm^3. It can be noticed that the density of the mineral MnO_2 is: $\rho_{MnO2} = 77.8/19.77 = 3.93$ and is closed to the density of MnOOH (ρ_{MnO2} = 4.31).